Highly selective ammonia gas sensor using Ga_2O_3/MoO_3 nanocomposite at ambient atmospheric conditions

Madhura N. Talwar [a], Asha P. Shirni [a], Rajendra Kumar R. T. [b], Gnana Prakash A. P [a,*]

[a] Department of Studies in Physics, University of Mysore, Manasagangothri, Mysuru 570 006, India
[b] Department of Nanotechnology, Bharathiar University, Coimbatore 641046, India

ARTICLE INFO

ABSTRACT

The β-Ga_2O_3 and MoO_3 nanocomposite with varying concentration of MoO_3 at 2.5 %, 5 % and 7.5 % were synthesized through hydrothermal method followed by physical mixing. Obtained nanocomposites were characterized to study its morphological, structural and optical properties through XRD, SEM, EDAX, TEM, XPS and UV–Visible spectroscopy. Surface area analysis was done using BET analysis method. Ammonia (NH_3) sensing studies were conducted at room temperature for synthesized composites. Nanocomposite with increased MoO_3 concentration showed increase in the response towards ammonia detection and highest response of 420.12 % for 100 ppm NH_3 at relative humidity (RH) of 69 % with response and recovery time of 53.75 s and 27.44 s respectively. Studies on humidity dependent sensing have been conducted for the same synthesized nanocomposites. The enhanced sensing of NH_3 in room temperature is attributed to sensing mechanism mediated by the adsorbed humidity and oxygen on the surface of the sensing material in addition to the chemical and electronic sensitization effects.

1. Introduction

Ammonia (NH_3) is a colorless gas with a pungent odor, widely recognized for its toxic and corrosive properties. The detection of ammonia (NH_3) is critical in various fields, including environmental monitoring, agriculture, and industrial safety, due to its toxicity and potential health hazards [1,2]. Exposure to ammonia can lead to a range of acute and chronic health effects, primarily affecting the respiratory system. Short-term exposure to high concentrations of ammonia can cause severe irritation of the eyes, nose, and throat, resulting in symptoms such as coughing, wheezing and difficulty breathing [3,4]. In more severe cases, ammonia exposure can lead to chemical burns on the skin and eyes, as well as pulmonary edema, which is a potentially life-threatening condition characterized by fluid accumulation in the lungs [5–7]. Since 16–28 % of the ammonia gas concentration in the atmosphere is thought to be lethal, proper monitoring of the gas concentration is essential for a healthy environment [8,9]. Therefore, it is important for both academia and industry to create effective gas sensors that can detect NH_3 at room temperature at lower concentrations (100 ppm). Typically, a variety of techniques were used to detect hazardous gases, such as gas chromatography, optical spectroscopy,

electrochemical methods, and semiconductors [10–13]. Because of their sophisticated sensing response to different gases, transition metal oxide semiconductor gas sensors were shown to be more efficient and cost-effective than other methods [14–16].

Among the other transparent conducting materials, gallium oxide (Ga_2O_3) has gathered significant attention in the field of gas sensing due to its remarkable properties and versatility. It has wide bandgap (ranging from approximately 4.2 to 5.2 eV) and depending on its crystalline phase, Ga_2O_3 exhibits excellent electrical and optical characteristics that make it suitable for various sensing applications [17,18]. The β-Ga_2O_3 is the most stable phase, is particularly noteworthy for its potential in high-temperature gas sensing, as it maintains structural integrity and functionality even in harsh environments [19,20]. The sensitivity of Ga_2O_3 to various gases, including oxygen, ammonia, and nitrogen dioxide, is a key factor that underpins its role as a gas sensor. This sensitivity can be enhanced through the engineering of defects and the introduction of dopants, which modify the electronic properties of the material. For instance, doping Ga_2O_3 with tin has been shown to improve its conductivity and gas sensing performance, allowing for more accurate detection of target gases [21]. Furthermore, the nano structuring of Ga_2O_3, such as the formation of nanowires or

nanoparticles, increases the surface area-to-volume ratio, thereby enhancing the interaction with gas molecules and improving sensor response times [22,23]. **Recent advancements in metal oxide–based gas sensors have demonstrated that surface modification, heterostructure formation, and humidity-assisted adsorption processes can significantly enhance gas sensing performance [24–27].** The composite formation of Ga_2O_3 with other materials can lead to synergistic effects that further enhance gas sensing capabilities. For example, composites of Ga_2O_3 with MWCNTs or other metal oxides can result in improved selectivity and sensitivity, making them suitable for detecting low concentrations of gases [28–30].

MoO_3, on the other hand, is recognized for its versatile crystalline phases and high reactivity, which contribute to its effectiveness in gas sensing [27]. A variety of gases, such as nitrogen dioxide, ammonia, and volatile organic compounds (VOCs), can be detected using MoO_3 because to its exceptional electrical conductivity and stability [31–33]. The material is more applicable in real-world situations where energy efficiency is crucial because of its capacity to operate efficiently at comparatively low operating temperatures [34]. Abdullah et al., has fabricated the SnO_2 coated Ga_2O_3 nanobelt for H_2 gas sensor. According to the obtained results, authors concludes that the SnO_2-coated Ga_2O_3 gas sensor operates at room temperature up to 200 °C and has a reversible response to a wide range of H_2 concentrations (33–1000 ppm) with low power consumption [35].

The integration of Ga_2O_3 and MoO_3 into a single nanocomposite represents a promising advancement in the field of gas sensor technology, particularly for the detection of ammonia (NH_3). Both materials exhibit unique properties that, when combined, can enhance the sensitivity and selectivity of gas sensors. The gas sensing mechanism of Ga_2O_3 and MoO_3 is primarily based on their interaction with gas molecules, leading to changes in their electrical resistance. When exposed to NH_3, these metal oxides undergo surface reactions that alter their charge carrier concentration, resulting in measurable changes in conductivity [36,37]. **The** Table 1 **presents the list of different chemiresistive NH_3 gas sensors fabricated using different nanoparticles along with their sensing parameters.**

In the present work the hydrothermally synthesized β-Ga_2O_3 along with the different percentages of MoO_3 (2.5 %, 5 % and 7.5 %) was used to study the gas sensing property towards NH_3 gas. The composite material was also tested under different relative humidity (RH) condition under room temperature (RT).

2. Experimental details

2.1. Synthesis of Ga_2O_3/MoO_3 nanocomposite

The hydrothermal process was used to synthesize the Ga_2O_3 and MoO_3 nanoparticles. First, 20 ml of deionized (DI) water is used to dissolve 0.51 g of Gallium (III) Nitrate Hydrate (Ga $(NO_3)_3$·nH_2O) and 0.116 g of Sodium Dodecyl Sulphate (SDS), which are then agitated for 20 min. Using 1 N NaOH (0.4 g NaOH in 10 ml of nano-pure water), the

pH of the above-prepared solution was kept at 10 while stirring continuously for an hour. After that, the mixture was put into a Teflon-coated autoclave and heated to 120 °C for 12 h, producing a white precipitate of gallium oxide hydroxide (GaOOH). The sample was then cooled and repeatedly cleaned with alcohol and DI water before being dried for five hours at 70 °C in an oven. The β-Ga_2O_3 nanoparticles were subsequently created by calcining the resultant powder for three hours at 1000 °C.

In order to synthesize MoO_3 nanoparticles, 0.392 g of Ammonium Molybdate $((NH_4)_2MoO_4)$ was dissolved in 10 ml of DI water. The solution was vigorously stirred for 15 min, and then 5 ml of concentrated HNO_3 was added and stirred for 1 h. The solution is transferred to autoclave at 180 °C for 24 h. Collected and washed product was calcinated at 500 °C for 2 h to obtain MoO_3 nanoparticles.

The obtained pristine materials were mixed in different weight ratio of 2.5 %, 5 % and 7.5 % by grinding them in mortar pestle to get the desired composite material.

2.2. Gas sensing measurements

Detailed fabrication process of gas sensor is described in our previous work [34]. The obtained nanocomposites along with the 50 µl NMP is mixed well and coated on IDEs as shown in Fig. 1. The gas sensing measurements were taken with the help of Keysight B2912A instrument in indigenously built set up for measuring sensing results. Synthetic air is used as a reference and diluting gas throughout the experiment.
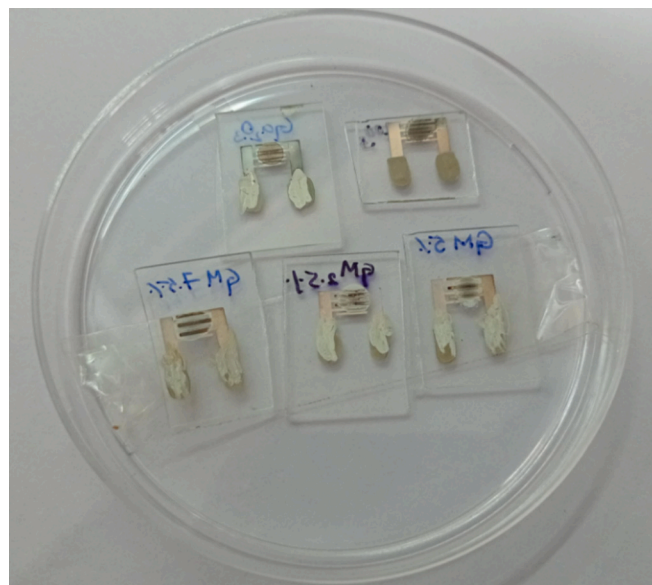

Fig. 1. Ga_2O_3/MoO_3 nanocomposite coated on Au IDEs.

Table 1
Chemiresistive NH_3 gas sensor for different materials.

Sensor Material	Working temperature (°C)	Sensing response	Response time (T_{res}) *sec*	Recovery time (T_{rec}) sec	NH_3 concentration (ppm)	References
Ga_2O_3/MoO_3	**RT**	**420.12 %**	**53.75**	**27.44**	**100**	**Present work**
ZnO	RT	52 %	49	59	50	[38]
h-MoO_3	200	36 %	230	267	5	[39]
Ga_2O_3	RT	160 %	42	30	100	[40]
$PtNps@TiO_2–WO_3$	RT	92.28	23	8	50	[41]
Polypyrrole/zinc-porphyrin	RT	104.3 %	42	223	1000	[42]
Sn doped Ga_2O_3	RT	274.98 %	–	–	200	[43]
MoS_2/WO_3	200	207 %	80	70	200	[44]
In_2O_3/Ga_2O_3	400	238 %	18	90	200	[45]
ZnO/rGO	RT	10.96	153	79	50	[46]

3. Results and discussion

3.1. XRD analysis

The Fig. 2 shows the XRD result of synthesized nanocomposites which are recorded using Rigaku-minifex with copper source of 1.5406 Å wavelength. The crystallinity and homogeneity of the synthesized nanoparticles are confirmed by the strong and evident peaks in the pristine Ga_2O_3 and MoO_3 nanoparticles XRD patterns. The XRD data is analyzed using the HighScore Plus tool for all the pristine and nanocomposite samples. It was confirmed that the produced Ga_2O_3 nanoparticles matched ICDD No. 00–041-1103 and exhibited a stable monoclinic crystal structure [40]. The pristine MoO_3 has hexagonal crystal structure that matches the ICCD No. 00–021-0569 with lattice constants a = 10.5310 Å, b = 10.5310 Å, c = 14.8760 Å, $\alpha = \beta = 90^o$ and $\gamma = 120^o$ [47]. The nanocomposite with different concentration of MoO_3 showed the prominent peak of MoO_3 peak around 25.8 °**(marked as * in composite XRD graph)** confirming the presence of MoO_3 and the intensity of this peak increases with the increase in the concentration of MoO_3. The crystallite size of the pristine and nanocomposite samples was calculated using Scherrer formula. It was found to be 22.86 nm, 38.87 nm for pristine Ga_2O_3 and MoO_3 material respectively. The composite crystallite size for 2.5 %, 5 % and 7.5 % MoO_3/Ga_2O_3 composite was 39.56, 39.24 and 35.6 nm respectively.

3.2. Raman analysis

Raman spectroscopy was used to explore the structural characteristics of pristine Ga_2O_3, MoO_3 and their combined Ga_2O_3/MoO_3 nanocomposite. The Fig. 3 displays the Raman spectrum of pristine and nanocomposite material. Raman spectrum of pristine Ga_2O_3 showed several peaks mainly in the 140–750 cm^{-1} range, consistent with its monoclinic β-phase structure [48]. For MoO_3, the distinct Raman peaks at 123, 179, 222, 252, 399, 512, 689, 901, and 990 cm^{-1} were observed. These peaks reflect the well-known vibrational features of the α-MoO_3 phase [49]. The lower wavenumber peaks (123–252 cm^{-1}) are typically associated with lattice vibrations and bending of O–Mo–O bonds, while the strong peak at 990 cm^{-1} corresponds to the stretching of terminal Mo=O bonds. Peaks at 689 and 901 cm^{-1} are linked to the vibrations of bridging oxygen atoms between Mo centres [50]. **The peaks corresponding to MoO_3 are marked * in the Ga_2O_3/MoO_3 composite Raman spectra**. When both oxides were combined in the Ga_2O_3/MoO_3 nanocomposite, a slight shift in the peak position can be noticed. These changes suggest that there are interactions between Ga_2O_3 and MoO_3 at the structural level, possibly due to lattice strain or chemical bonding at the interface [51,52].
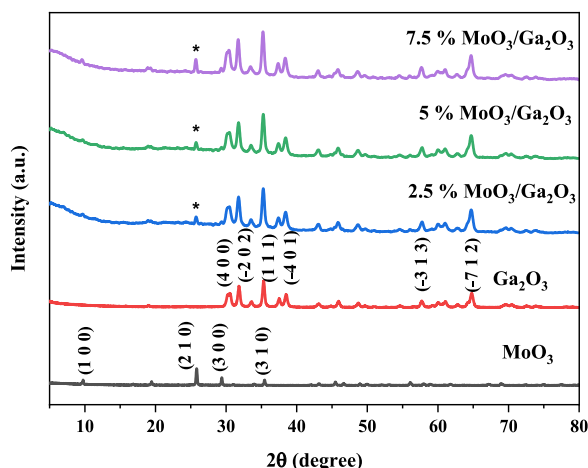

Fig. 2. XRD pattern of pristine Ga_2O_3, MoO_3 and $Ga_2O_3/$ MoO_3 nanocomposite.
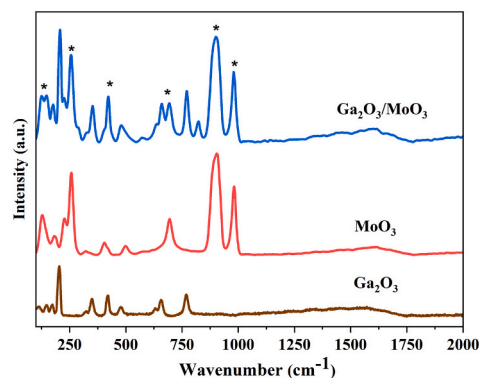
Fig. 3. Raman spectra of pristine Ga_2O_3, MoO_3 and $Ga_2O_3/$ MoO_3 nanocomposite.

3.3. Morphological and elemental analysis

The Fig. 4 shows the surface morphology of the synthesized Ga_2O_3/MoO_3 nanocomposite examined using SEM at various magnifications. The micrographs shed light on surface texture, particle dispersion, and nanostructure of the material. The SEM analysis confirms that the Ga_2O_3/MoO_3 nanocomposite consists of well-defined, densely packed nanorod like structures with uniform morphology. The porous texture and high surface area observed at lower magnifications are likely beneficial for gas-sensing applications [53]. The hierarchical structuring observed at different magnifications suggests that the synthesis approach effectively promoted the growth of nanostructured features with strong interfacial interactions between Ga_2O_3 and MoO_3.

The compositional analysis of Ga_2O_3/MoO_3 sample was performed using the EDS technique as shown in Fig. 5. The figure shows that the sample shows the peak corresponding to Ga, Mo and O with no other additional peaks indicating the purity and it is compatible with the XRD results. Further Fig. 6 presents the EDS mapping for the sample with 7.5 % MoO_3, showing the distribution of Ga, O and Mo.

The Fig. 7**(a-f)** exhibit the TEM images of Ga_2O_3/MoO_3 nanocomposite. The images in Fig. 7**(a-c)** shows the arrangement of rod like Ga_2O_3 and MoO_3 particles in the nanocomposite. A distinguished lattice fringes measuring 0.628 and 0.372 nm were observed in the Fig. 7**(d-e)** corresponding to Ga_2O_3 and MoO_3 respectively. The selective area electron diffraction (SAED) pattern of the synthesized sample is shown in Fig. 7f and it is in good agreement with the corresponding XRD pattern. The effective synthesis of a well-crystallized Ga_2O_3/MoO_3 nanocomposite with clear grain boundaries and high structural integrity is confirmed by TEM images.

3.4. Optical analysis

The UV–Vis absorption spectra of Ga_2O_3/MoO_3 nanocomposites with varying MoO_3 weight percentages 2.5 %, 5 %, and 7.5 % are displayed in Fig. 8(a). The UV–Vis absorption spectra of Ga_2O_3/MoO_3 nanocomposites demonstrate notable variations in their optical absorption behaviour. Wide bandgap semiconductors are characterized by a prominent absorption edge in the ultraviolet spectrum, which is present in all samples. However, a significant redshift in the absorption edge is seen as the MoO_3 content increases. The 7.5 % MoO_3 sample has the most noticeable red-shift, while the 2.5 % sample displays the absorption edge at a shorter wavelength. This shift indicates that the presence of more MoO_3 introduces changes in the electronic structure, possibly due to stronger interaction between the Ga_2O_3 and MoO_3 phases or the formation of defect states [54]. Additionally, the increase in overall absorbance with higher MoO_3 content suggests better light absorption capabilities, which could enhance the material's performance in applications like photocatalysis or sensing [55].
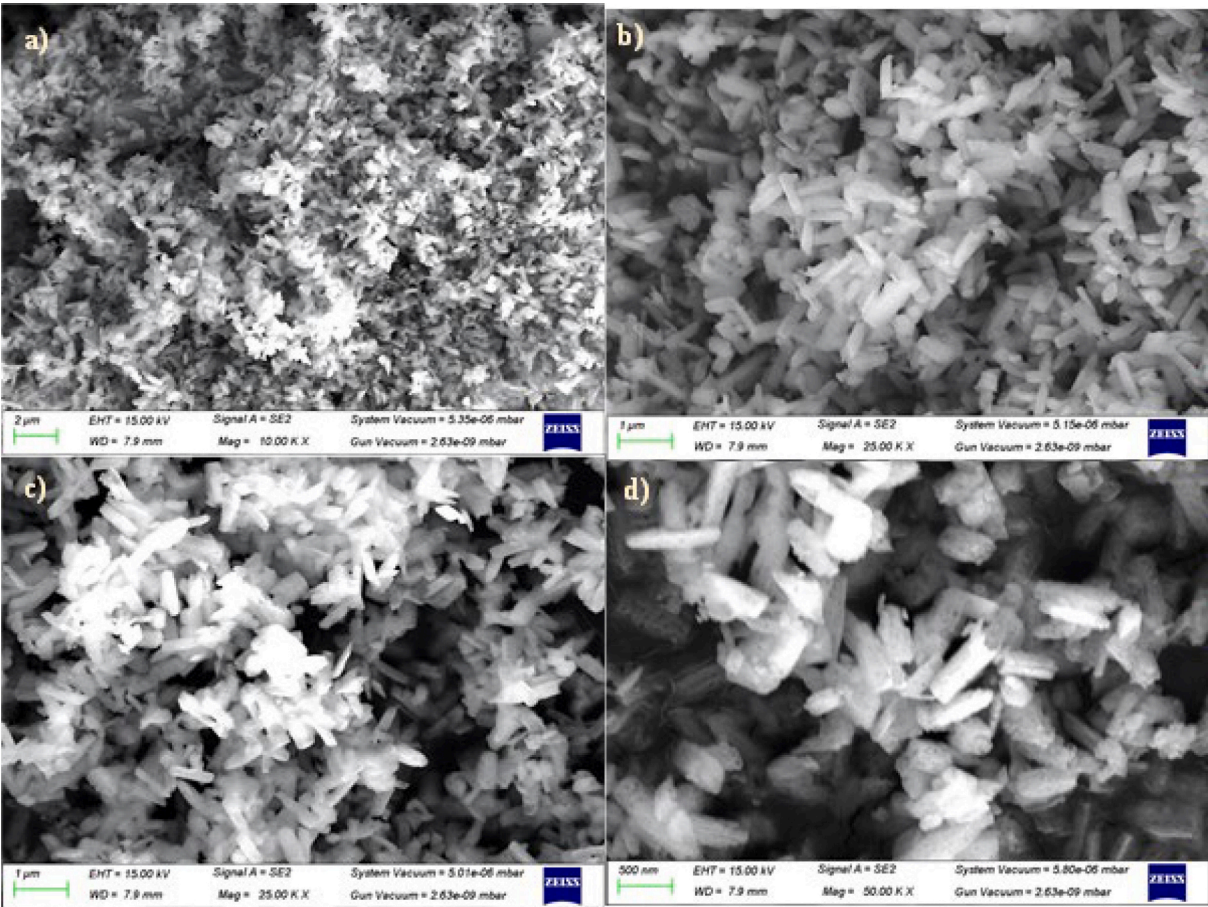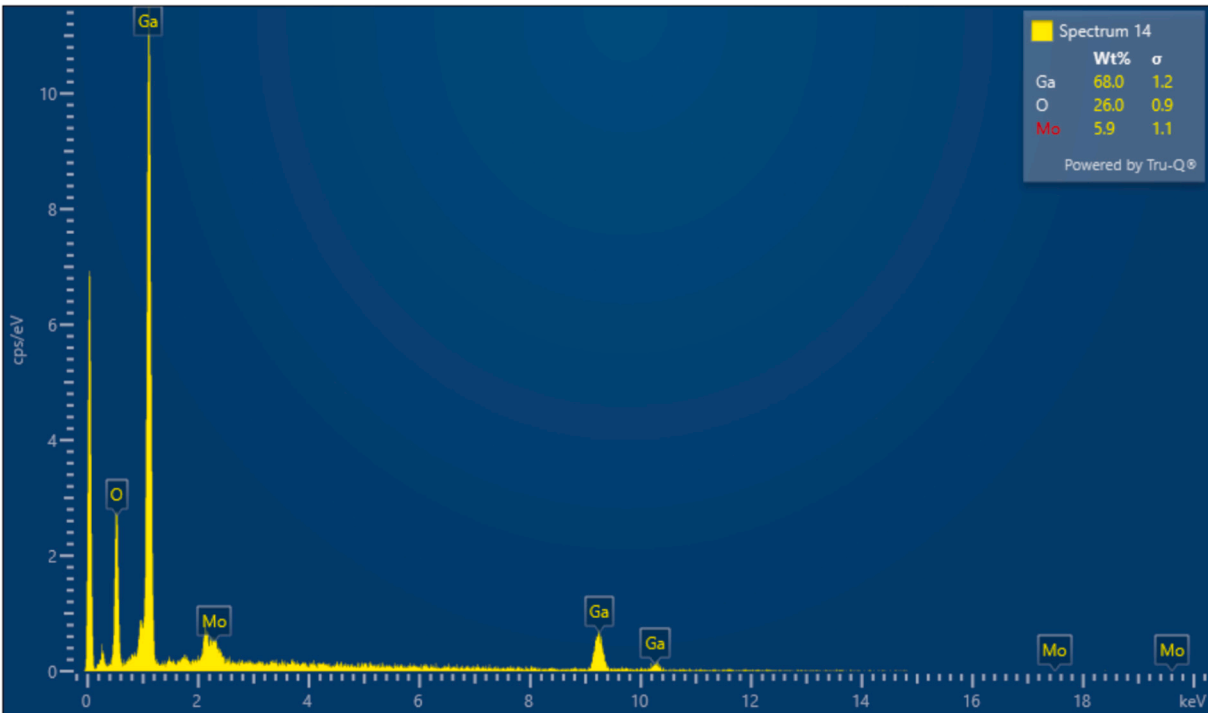
Fig. 4. SEM images of Ga_2O_3/MoO_3 nanocomposite.

Fig. 5. EDS spectrum of 7.5 % MoO_3/Ga_2O_3 nanocomposite.
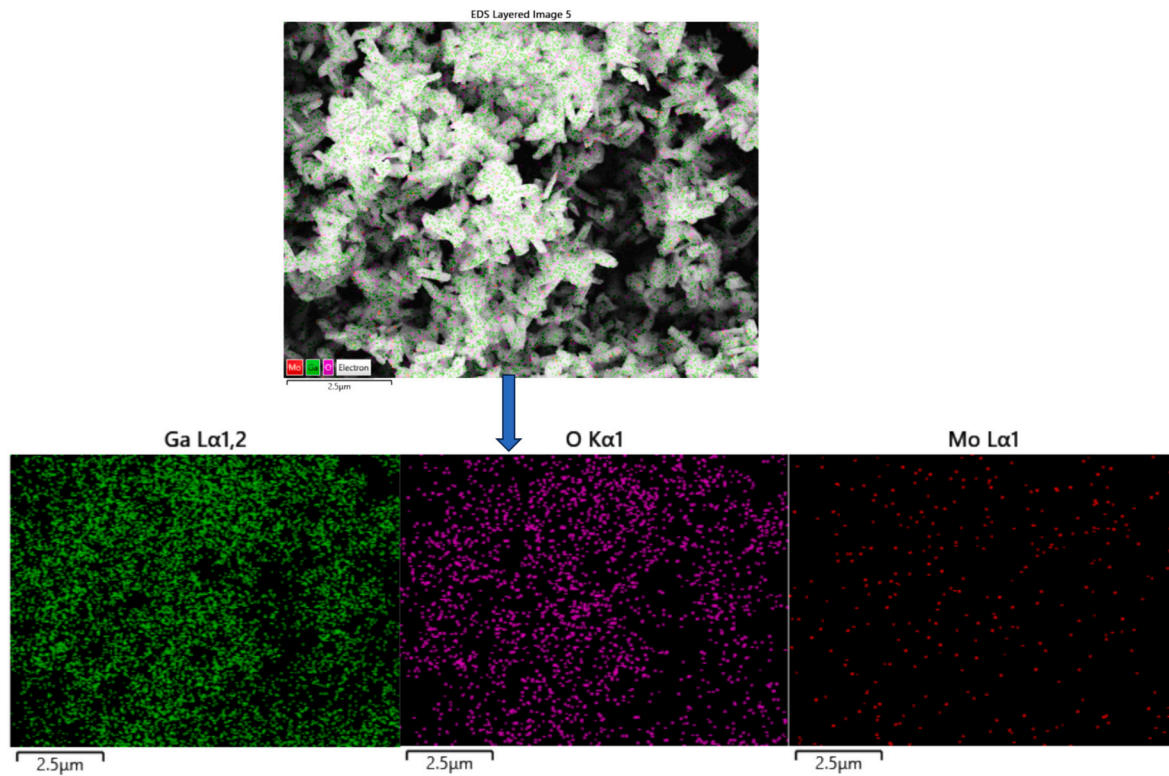
Fig. 6. EDS Elemental mapping of 7.5 % MoO_3/Ga_2O_3 nanocomposite.

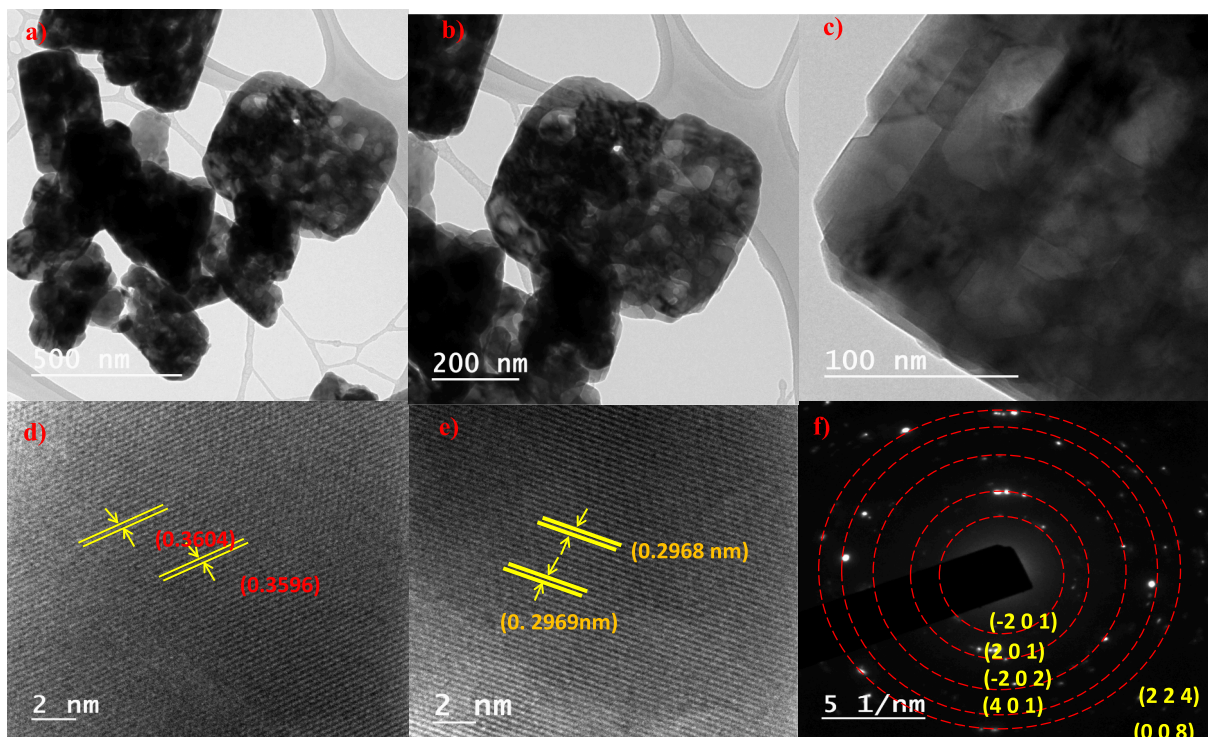**Fig. 7.** TEM images of Ga_2O_3/MoO_3 nanocomposite.

The bandgap energy was calculated by means of the Kubelka-Munk (K-M) algorithm and plot is given in Fig. 8(b). The bandgap energy of the composites was 2.86 eV, 2.63 eV and 2.41 eV for 2.5 %, 5 % and 7.5 % MoO_3 respectively. The 2.5 wt% MoO_3 sample shows the highest bandgap energy, while the 7.5 wt% sample exhibits the lowest. This red shift in the absorption edge suggests enhanced electronic interaction between Ga_2O_3 and MoO_3, possibly due to the introduction of defect states or modified electronic structure at the interface [56]. Based on these results, it is possible to effectively customize the optical characteristics of the composite for certain functional applications by adjusting
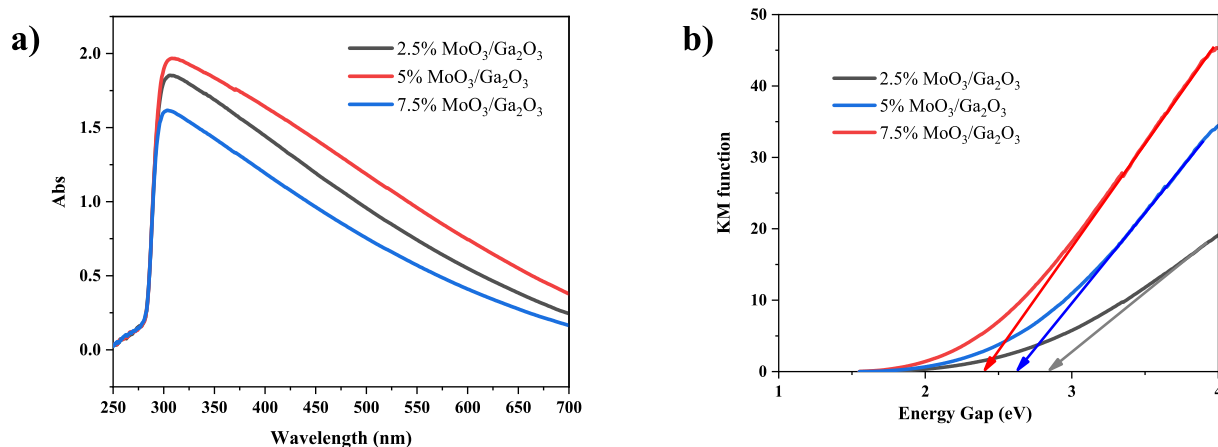
Fig. 8. a) Absorption spectra b) KM plot of Ga_2O_3/MoO_3 nanocomposite with 2.5 %, 5 % and 7.5 % MoO_3.

the concentration of MoO_3 in the composite.

3.5. XPS studies

The Fig. 9 shows the results of XPS characterisation, which was utilized to determine the composition and chemical bonding states of the composite under investigation. The composition with 7.5 % $MoO_3/$ Ga_2O_3 XPS survey spectra is presented in Fig. 9(a), where photoelectron spectra with Ga (3d, 3p, 3 s, 2p and LMM), Mo (3d), O (2 s, 1 s), and C (1 s) peaks have been identified [57,58].

The C—C bond at 284.3 eV from unexpected surface contamination serves as the calibration for all binding energies [47]. The Fig. 9(b) display the O—Ga bond for lattice O^{2-} ions is represented by the core level of O 1 s, which is located at 532.4 eV [59,60]. The peak at 21.5 eV
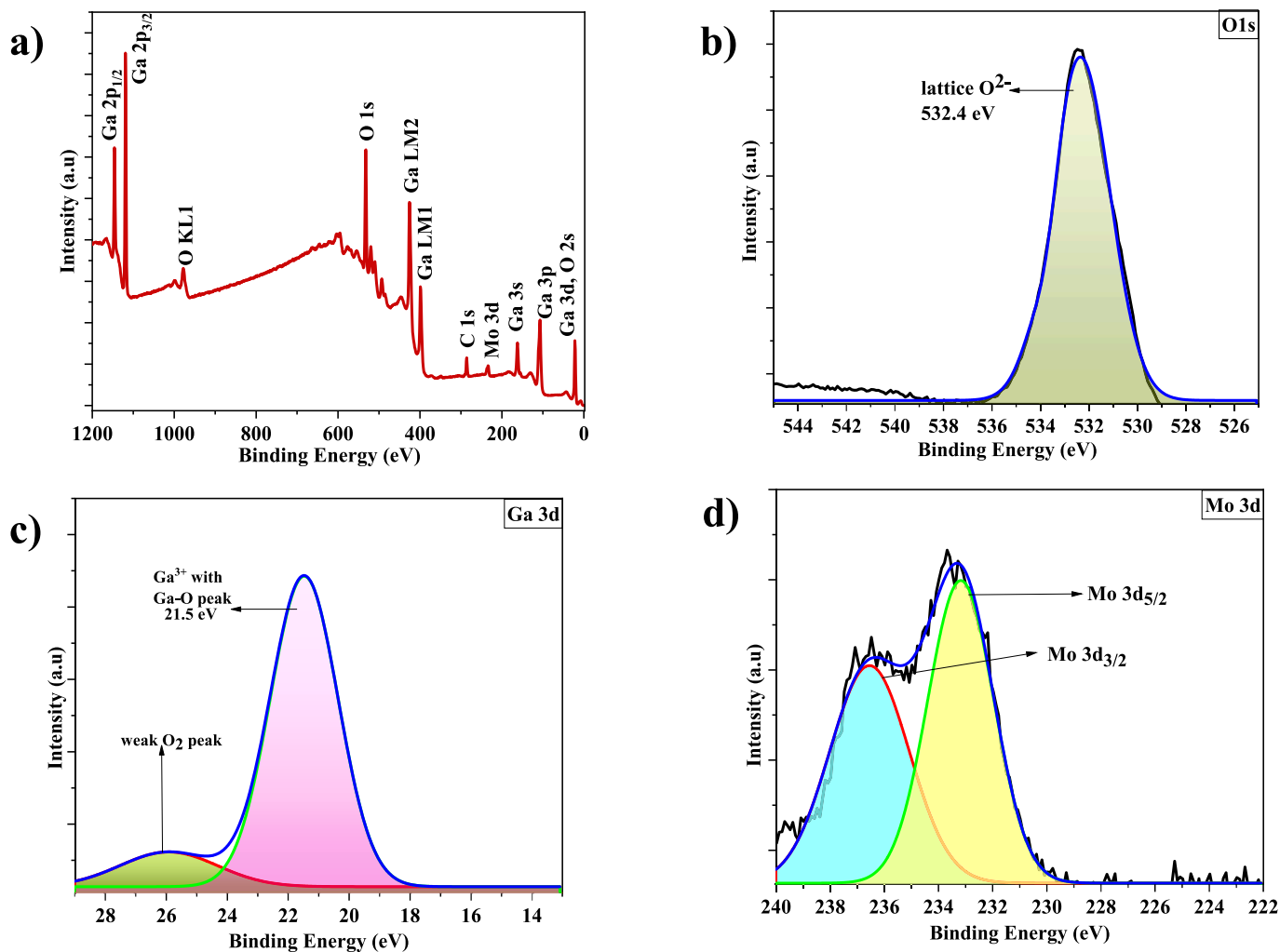

Fig. 9. XPS spectra of a) Ga_2O_3/MoO_3 nanocomposite b) O 1 s c) Ga 3d d) Mo 3d.

is attributable to the Ga 3d with Ga—O bond, is depicted in Fig. 9(c). In addition to the peak, a weak O 2 s peak can be observed at 26.05 eV [60–62]. The high resolution XPS spectra in Fig. 9(d) show doublet peaks that match to the molybdenum 3d state of the material at 233.2 eV and 236.5 eV, respectively, representing the $3d_{5/2}$ and $3d_{3/2}$ states [63,64].

3.6. Surface area analysis

The Ga_2O_3/MoO_3 nanocomposites is subjected to Brunauer-Emmett-Teller (BET) surface area analysis to study the surface features and the result is given in Fig. 10. The nitrogen adsorption–desorption isotherm of the Ga_2O_3/MoO_3 nanocomposite displays a type IV curve accompanied by an H3-type hysteresis loop, which is characteristic of mesoporous materials, typically formed by aggregates of plate-like particles [65–67]. A larger BET surface area of 253 m^2 g^{-1} and the pore volume $V_p = 0.55$ cm^3 g^{-1} implies that more active sites are available on the material's surface for gas molecule interaction, which is critical for enhancing sensor response and sensitivity [40,68,69].

The distribution of pore sizes is shown in the inset of Fig. 10, and it is clear that the Ga_2O_3/MoO_3 sample has a broad range of pore radii, peaking at RP = 19.65 nm. Additionally, the mesoporous framework enables efficient gas transport within the sensing layer, contributing to quicker response and recovery times. The integration of Ga_2O_3 and MoO_3 not only modifies the surface and electronic properties but also contributes to a porous architecture that supports better gas adsorption dynamics and charge transfer which are key parameters in high-performance gas sensors.

3.7. Gas sensing studies

Sensing experiments on Ga_2O_3/MoO_3 nanocomposites with varying concentrations of analyte gas were conducted at RT by subjecting the sensor coated films, made using the drop casting technique. The sensing chamber, which is coupled to a high resistance electrometer, was used to expose sensor films to NH_3 vapours at different concentrations. The resistant the sensor film was noted in the ambient environment prior to injecting analyte vapours. Specific concentration of NH_3 vapours injected into the chamber and the variation of the sensor resistance was measured. The eq. (1) was used to compute the film's sensing responses to various NH_3 concentrations, in increments of 20 ppm from 10 ppm to 100 ppm.

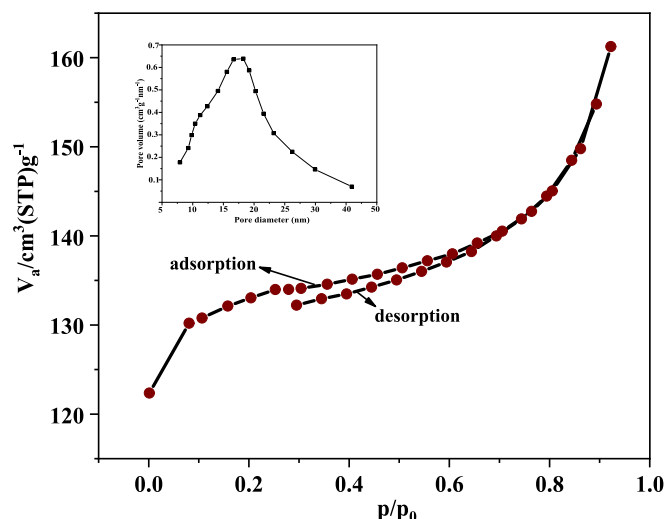$$S\% = \frac{I_a - I_g}{I_a} \tag{1}$$

where "S" denotes the sensing response, "$I_a^{''}$" is the current flowing through the film in atmospheric air, and "$I_g^{''}$" denotes the current when NH_3 is present. The sensor response was calculated for 2.5 %, 5 % and 7.5 % weight percentage concentration of MoO_3 in the composite. The results indicate that the pristine Ga_2O_3 provides better response to NH_3 gas when compared to pristine MoO_3, with the addition of low wt% (2.5 %, 5 %) MoO_3 to Ga_2O_3 a slight increase in the response was observed. The composite with 7.5 % MoO_3/Ga_2O_3 showed the highest response of 420.12 % indicating that combined effect of Ga_2O_3 and MoO_3 contribution in detecting the NH_3 vapours and the optimal mixing parameters for a porous mixture to achieve a successful Ga_2O_3/MoO_3 interaction [70]. Therefore, in comparison to pristine Ga_2O_3 and MoO_3 based sensors, the Ga_2O_3/MoO_3 nanocomposite sensor has a higher gas detection response and it is shown in Fig. 11. The study was repeated at room temperature with different RH values and results were plotted.

The response and recovery time for the 7.5 % MoO_3/Ga_2O_3 composite is shown in Fig. 12 for 100 ppm of NH_3 gas. The response time is defined as the time for the sensor to reach 90 % of its maximum response after gas exposure, while the recovery time is defined as the time taken for the sensor to return to 90 % of its initial resistance after the gas is removed. The sensor demonstrated rapid performance, achieving a response time of 57.35 s when exposed to the target gas and recovering in 27.44 s after the gas was removed. These swift response and recovery characteristics indicate that the sensor is highly suitable for real-time applications.

3.8. The sensor's selectivity and sensitivity

The Fig. 13a displays the 7.5 % MoO_3/Ga_2O_3 sensor on/off cycles for 100 ppm of NH_3 gas at room temperature with 69 % relative humidity. The sensor's reaction is steady and reversible, as illustrated in the figure. The response of the sensor to varying concentrations in increments of 20 ppm is shown in Fig. 13b. A response of 33.3 % was noted towards 20 ppm of NH_3, indicating the good sensitivity of the synthesized nanocomposite-based sensor. The Fig. 13c illustrates the linear relationship between the sensor response for varying NH_3 concentrations. According to the slope of the linear line, the sensor's sensitivity is 5.03 %/ppm, which is defined as the change in current response per 1 ppm of analyte gas [71]. In contrast to the other gases employed in the studies, the synthesized sensor shows strong selectivity to NH_3, as determined by the selectivity study shown in Fig. 13d. The 7.5 wt% MoO_3 sensor was subjected to a selectivity test at RH with 69 % RH using 500 ppm concentrations of propanol, ethanol, toluene, formaldehyde, and acetone.
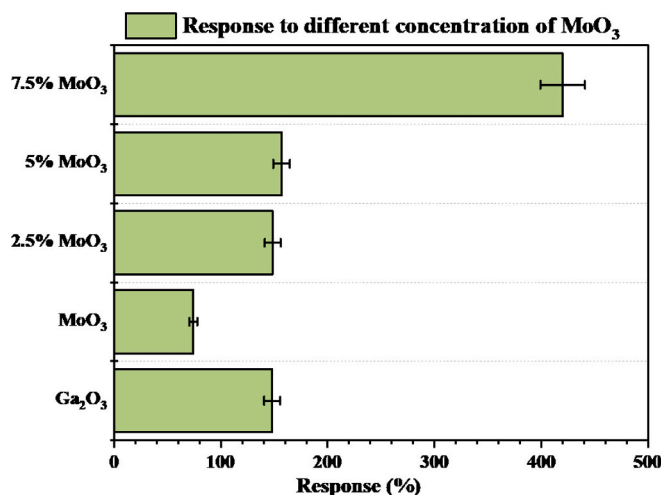

Fig. 10. BET analysis of Ga_2O_3/MoO_3 nanocomposite.

Fig. 11. Current Response of the pristine Ga_2O_3, MoO_3 and Ga_2O_3/MoO_3 with different concentration.
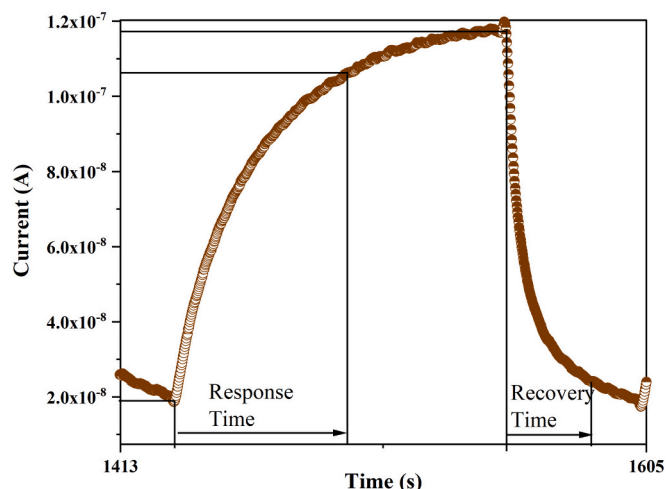
Fig. 12. Response and recovery time of 7.5 % MoO_3/Ga_2O_3 composite sensor for 100 ppm NH_3.
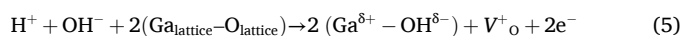
3.9. Sensing mechanism

Humidity is the main obstacle for the majority of semiconducting metal oxide gas sensors at room temperature because it interacts with the sensing material surface and restrict the sensing capability leading to the degradation of its performance [72]. Whereas according to reports, β-Ga_2O_3 is a potential option for room temperature humidity sensing applications [28,73]. Additionally, at room temperature, NH_3 and H_2O react and enhance the sensing property. These two facts suggest two

potential modules of mechanisms based on adsorbed oxygen and humidity-assisted NH_3 sensing pathways.

3.9.1. Humidity assisted sensing

At room temperature, humidity assisted detection of NH_3 vapours starts with the dissociative adsorption of H_2O as H^+ and OH^- on the surface of metal oxides, as shown in eq. (4). The ambient environment during sensing experiment refers to the wet environment with minimal humidity levels, where in one can assume that adsorption of one H_2O molecule led to two adsorption active sites [74]. According to eq. (5), this dissociative adsorption causes the lattice to create an oxygen vacancy and a $Ga^{\delta+} - OH^{\delta-}$ dipole. As seen in eq. (6), further interaction between H_2O and these dipoles creates a liquid electrolyte medium, where NH_3 undergoes electrolytic dissociation to yield NH^{4+} and OH^-. This electrolytic dissociation of NH_3 causes variations in ionic and electronic conduction on sensing material surface, which in turn causes variations in the electronic output.

$$H_2O \rightarrow H^+ + OH^- \tag{4}$$

$$H^+ + OH^- + 2(Ga_{lattice}-O_{lattice}) \rightarrow 2 (Ga^{\delta+} - OH^{\delta-}) + V^+{}_O + 2e^- \tag{5}$$

$$NH_3 + H_2O \rightarrow NH_4^+ + OH^- \tag{6}$$

3.9.2. Sensing by adsorbed oxygen

Both Ga_2O_3 and MoO_3 are n-type semiconductors, on exposure to air, ionized oxygen species (O_2^-) can adsorb onto their surfaces and capture free electrons as shown in eq. (7), leading to the formation of a depletion layer near the surface. This process increases the resistance of the material. Upon exposure to NH_3, the gas molecules interact with the adsorbed oxygen species. NH_3 acts as a reducing agent, donating
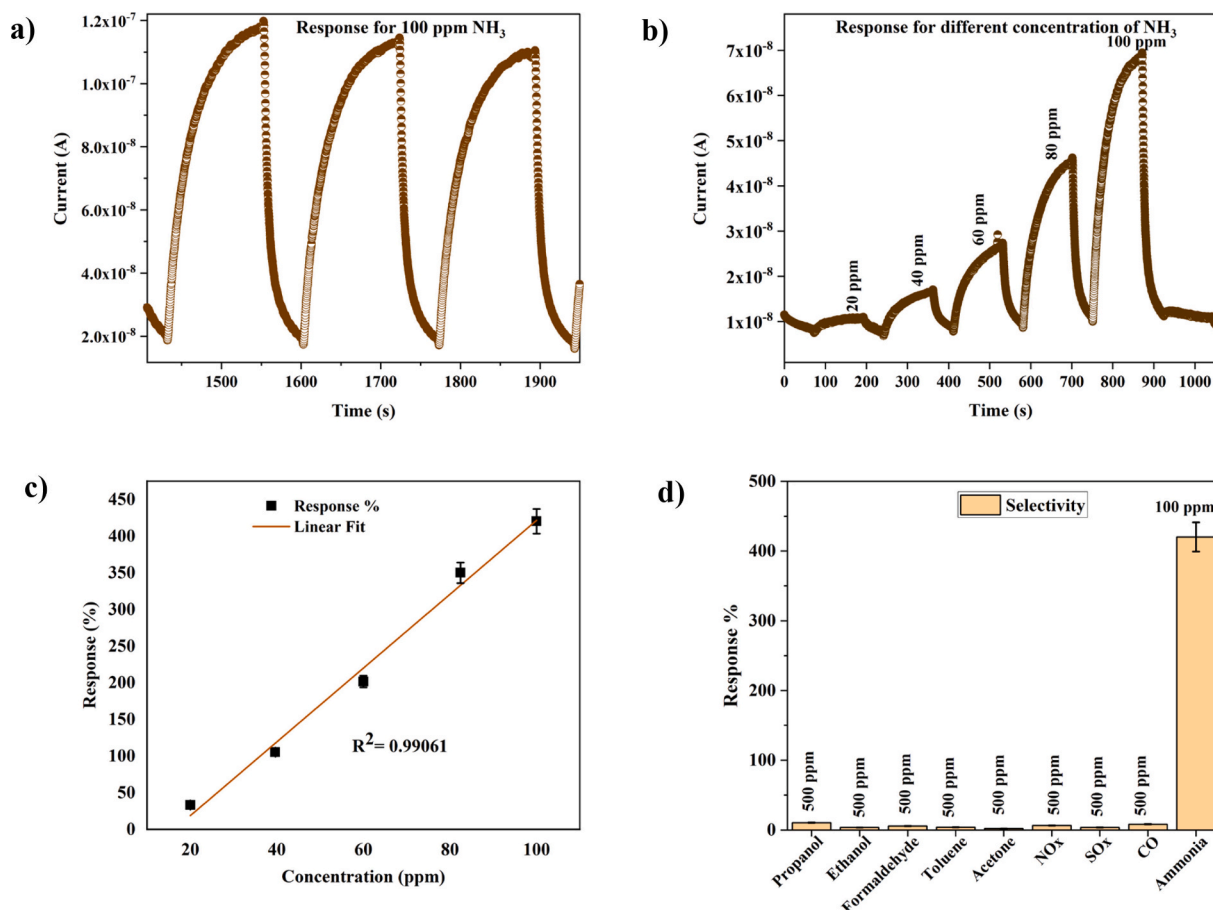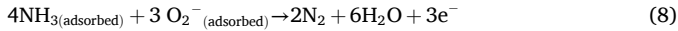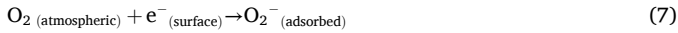

Fig. 13. a) Sensor response b) Sensitivity c) Linearity d) Selectivity of Ga_2O_3/MoO_3 composite.

electrons to the semiconductor surface (eq. (8)). This interaction reduces the depletion layer's width, effectively lowering the resistance of the material and allowing for gas detection [75–77].

$$O_{2\ (atmospheric)} + e^-_{(surface)} \rightarrow O_2^-_{(adsorbed)} \tag{7}$$

$$4NH_{3(adsorbed)} + 3\ O_2^-_{(adsorbed)} \rightarrow 2N_2 + 6H_2O + 3e^- \tag{8}$$

The spilling effect of adding MoO_3 over the surface increases the chances that reactive oxygen or hydroxyl species will be adsorbed on the composite surface, providing more active sites for adsorption that could accelerate the kinetics of surface chemical processes [78,79]. The various methods that improve the NH_3 sensing capabilities of Ga_2O_3/MoO_3 composite in comparison to pristine Ga_2O_3 at RT as shown in Fig. 14(a, b).

3.10. Humidity variation study

The response of 7.5 % MoO_3/Ga_2O_3 nanocomposite sensor with varying RH from 56 % to 80 % for 100 ppm of NH_3 was studied and the results are given in Fig. 15. It can be seen from that with increased RH the response of the sensor increases displaying maximum response at 69 % RH. Further increase in the RH decreases the response considerably. Research indicates that there exists an optimal humidity level where gas sensitivity is maximized without excessive interference. While low humidity may provide weak adsorption of NH_3, excessively high humidity can lead to saturation and poor response due to the predominant adsorbate being water rather than the target gas itself. Therefore, increase in the humidity beyond optimal 69 % will considerably decreases the response of the sensor [28,73,76].
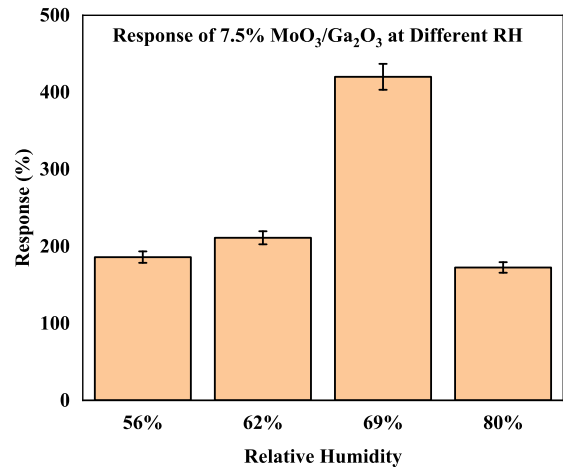

Fig. 15. Humidity study of Ga_2O_3/ MoO_3 composite.

3.11. Conclusion

NH_3 gas detection using a room temperature sensor based on Ga_2O_3/MoO_3 nanocomposites has been extensively researched. To synthesize Ga_2O_3 and MoO_3 nanoparticles, a hydrothermal method was used. Through physical mixing of pristine samples at different weight ratios in NMP, the Ga_2O_3/MoO_3 nanocomposites were produced. The addition of MoO_3 alters the sensor's response to NH_3 gas. The addition of MoO_3 content is between 2.5 and 5 wt% shows a slight increase in the response of the sensor whereas to 7.5 wt% the response increase rapidly indicating that combined effect of Ga_2O_3 and MoO_3 contribution in detecting the NH_3 vapours implying the ideal mixing conditions for a porous
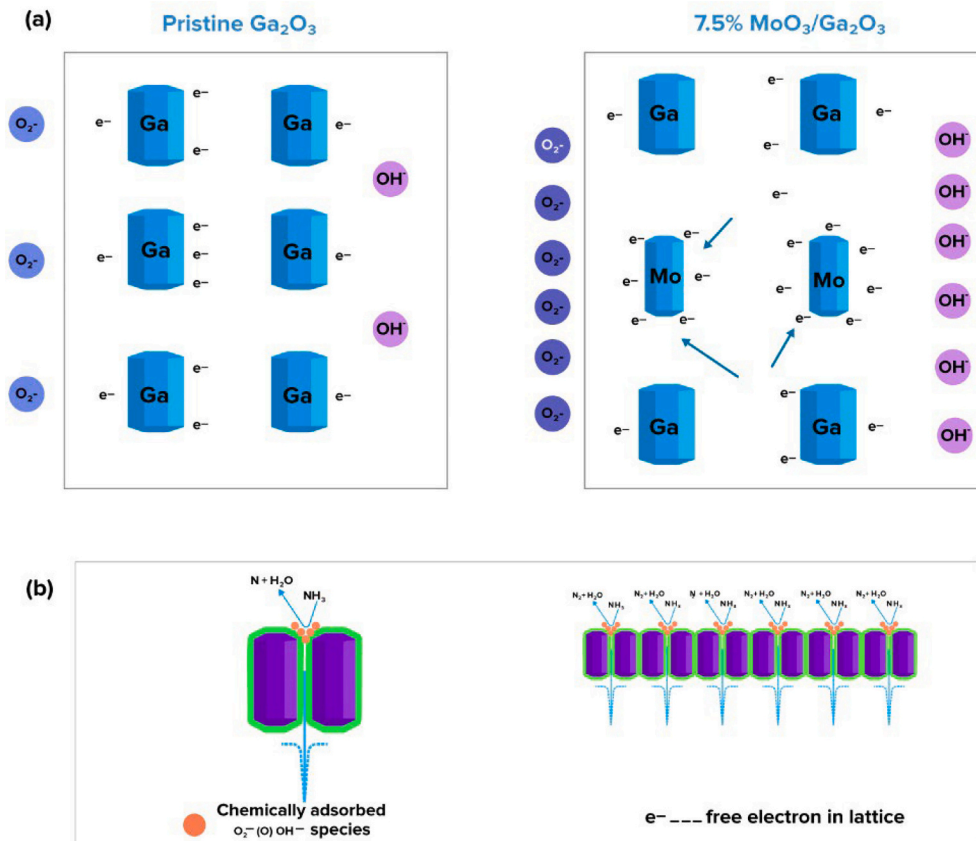

Fig. 14. Sensing mechanism of Ga_2O_3/MoO_3 for NH_3 detection a) adsorption oxygen and hydroxyl species b) electron and ionic conduction.

combination for effective Ga_2O_3/MoO_3 interaction. The sample with Ga_2O_3 and 7.5 wt% MoO_3 exhibits maximum response (420.12 % for 100 ppm NH_3) in RT at RH 69 %. The superior sensing performance can be attributed to the reduced crystallite size, enlarged surface area and higher surface-to-volume ratio, along with the development of a rod like morphology, all of which provide more active sites for gas adsorption and facilitate efficient charge transport. In addition, the sensor displays excellent selectivity for NH_3 when compared to other volatile organic compounds.

CRediT authorship contribution statement

Madhura N. Talwar: Writing – review & editing, Writing – original draft, Visualization, Resources, Methodology, Investigation, Formal analysis, Data curation. **Asha P. Shirni:** Formal analysis, Data curation. **Rajendra Kumar R. T.:** Validation, Resources, Data curation. **Gnana Prakash A. P:** Supervision.

Declaration of competing interest

The authors declare that they have no known competing financial interests or personal relationships that could have appeared to influence the work reported in this paper.

Acknowledgement

Data availability

Data will be made available on request.

References

[1] M.J. Fedoruk, R. Bronstein, B.D. Kerger, Ammonia exposure and hazard assessment for selected house hold cleaning product uses, J. Exposure Anal. Epidomiol. 15 (2005) 534, https://doi.org/10.1038/sj.jea.7500431.

[2] Lalit Kumar, Ishpal Rawal, Amarjeet Kaur, S. Annapoorni, Flexible room temperature ammonia sensor based on polyaniline, Sensors Actuators 240 (2017) 408, https://doi.org/10.1016/j.snb.2016.08.173.

[3] Diana, et al., Why it is often underestimated: historical study of Ammonia gas exposure impacts towards human health, E3s web of conferences (2018), https://doi.org/10.1051/e3sconf/20187306003.

[4] Gafor "utilizing wind rose information for the prediction of Ammonia migration", International journal of academic research in business and social sciences (2023) https://doi.org/10.6007/ijarbss/v13-i15/18789.

[5] Liu, et al., Ammonia induce lung tissue injury in broilers by activating NLRP3 inflammasome via Escherichia/Shigella, Poult. Sci. (2020) https://doi.org/10.1016/j.psj.2020.03.019.

[6] B. Das, S. Kumar, S.P. Sivapirakasam, Risk and consequence analysis of ammonia storage units in a nuclear fuel cycle facility, Process. Saf. Prog. 43 (4) (2024) 668–677.

[7] L. Zhihua, Z. Xucheng, S. Jiyong, Z. Xiaobo, H. Xiaowei, H.E. Tahir, M. Holmes, Fast response ammonia sensor based on porous thin film of polyaniline/sulfonated nickel phthalocyanine composites, Sensors Actuators B Chem. 226 (2016) 553, https://doi.org/10.1016/j.snb.2015.10.062.

[8] M. Poloju, N. Jayababu, M.V. Ramana Reddy, Improved gas sensing performance of Al doped ZnO/CuO nanocomposite-based ammonia gas sensor, Mater. Sci. Eng. B Solid-State Mater. Adv. Technol. 227 (2018) 61–67, https://doi.org/10.1016/j.mseb.2017.10.012.

[9] B. Timmer, W. Olthuis, A. Van Den Berg, Ammonia sensors and their applications - a review, Sensors Actuators B Chem. 107 (2005) 666–677, https://doi.org/10.1016/j. snb.2004.11.054.

[10] J.L. Little, A.S. Howard, Qualitative gas chromatography-mass spectrometry analyses using amines as chemical ionization reagent gases, J. Am. Soc. Mass Spectrom. 24 (2013) 1913–1918, https://doi.org/10.1007/s13361-013-0740-8.

[11] V.M.N. Passaro, F. Dell'Olio, F. De Leonardis, Ammonia optical sensing by microring resonators, Sensors 7 (2007) 2741–2749, https://doi.org/10.3390/s7112741.

[12] E. Bakker, M. Telting-diaz, Electrochemical Sesnors, Anal. Chem. 74 (2002) 2781–2800, https://doi.org/10.1021/ac060637m.Electrochemical.

[13] M.B. Rahmani, S.H. Keshmiri, J. Yu, A.Z. Sadek, L. Al-Mashat, A. Moafi, K. Latham, Y.X. Li, W. Wlodarski, K. Kalantar-zadeh, Gas sensing properties of thermally

[14] N. Jayababu, M. Poloju, M.V. Ramana Reddy, Facile synthesis of SnO2-Fe2O3 core/shell nanostructures and their 2-methoxyethanol gas sensing characteristics, J. Alloys Compd. 780 (2019) 523–533, https://doi.org/10.1016/j.jallcom.2018.11.413.

[15] M. Poloju, N. Jayababu, E. Manikandan, M.V. Ramana Reddy, Enhancement of the isopropanol gas sensing performance of SnO2/ZnO core/shell nanocomposites, J. Mater. Chem. C 5 (2017) 2662–2668, https://doi.org/10.1039/c6tc05095f.

[16] T. Gao, T.H. Wang, Synthesis and properties of multipod-shaped ZnO nanorods for gas-sensor applications, Appl. Phys. A Mater. Sci. Process. 80 (2005) 1451–1454, https://doi.org/10.1007/s00339-004-3075-2.

[17] N. Ma, N. Tanen, A. Verma, Z. Guo, T. Luo, H.G. Xing, D. Jena, Intrinsic electron mobility limits in β-Ga2O3, Appl. Phys. Lett. 109 (21) (2016).

[18] M. Mishra, S.K. Tc, N. Aggarwal, M. Kaur, S. Singh, G. Gupta, Pit assisted oxygen chemisorption on GaN surfaces, Phys. Chem. Chem. Phys. 17 (23) (2015) 15201–15208.

[19] U. Hoefer, J. Frank, M. Fleischer, High temperature Ga2O3-gas sensors and SnO2-gas sensors: a comparison, Sensors Actuators B Chem. 78 (1–3) (2001) 6–11.

[20] M. Bartic, C.I. Baban, H. Suzuki, M. Ogita, M. Isai, B-Gallium oxide as oxygen gas sensors at a high temperature, J. Am. Ceram. Soc. 90 (9) (2007) 2879–2884.

[21] N.S. Jamwal, A. Kiani, Gallium oxide nanostructures: A review of synthesis, properties and applications, Nanomaterials 12 (12) (2022) 2061.

[22] S.P. Arnold, S.M. Prokes, F.K. Perkins, M.E. Zaghloul, Design and performance of a simple, room-temperature Ga2O3 nanowire gas sensor, Appl. Phys. Lett. 95 (10) (2009).

[23] S. Kumar, R. Singh, Nanofunctional gallium oxide (Ga2O3) nanowires/nanostructures and their applications in nanodevices, physica status solidi (RRL)–Rapid Research Letters 7 (10) (2013) 781–792.

[24] J. Hu, X. Liu, J. Zhang, X. Gu, Y. Zhang, Plasmon-activated NO2 sensor based on au@ MoS2 core-shell nanoparticles with heightened sensitivity and full recoverability, Sensors Actuators B Chem. 382 (2023) 133505.

[25] J. Hu, X. Wang, H. Lei, M. Luo, Y. Zhang, Plasmonic photothermal driven MXene-based gas sensor for highly sensitive NO2 detection at room temperature, Sensors Actuators B Chem. 407 (2024) 135422.

[26] J. Hu, Y. Zhao, Q. Wang, Y. Zhang, Full-Spectrum Visible Light Driven Chemiresistive Sensor Based on g-C3N4/SnS/au Heterostructures for Reliable NO2 Detection at Room Temperature, Sensors Actuators B Chem. 442 (2025) 138103.

[27] J. Hu, Y. Zhao, B. Liu, Y. Zhang, Indoor white light activated NO2 sensor based on au@ MoS2/SnS nanocomposites with enhanced responsiveness at room temperature, Sensors Actuators B Chem. 433 (2025) 137556.

[28] M.N. Talwar, A. Gangadhar, M. Manoharan, R. Manimozhi, S. Srikantaswamy, R. R. Kumar, A.G. Prakash, Humidity enhanced ammonia gas sensing by Ga2O3/MWCNT nanocomposite at room temperature, Mater. Sci. Semicond. Process. 175 (2024) 108255.

[29] J. Ahmed, M. Faisal, J.S. Algethami, M.M. Rahman, F.A. Harraz, A novel Ga2O3-doped ZnO decorated SWCNT nanocomposite based amperometric sensor for efficient detection of dopamine in real samples, J. Sci.: Adv. Mater. Devices 9 (1) (2024) 100668.

[30] O. Lupan, T. Braniste, M. Deng, L. Ghimpu, I. Paulowicz, Y.K. Mishra, I. Tiginyanu, Rapid switching and ultra-responsive nanosensors based on individual shell–core Ga2O3: ox@ SnO2 nanobelt with nanocrystalline shell in mixed phases, Sensors Actuators B Chem. 221 (2015) 544–555.

[31] M.G. da Silva Júnior, L.C.C. Arzuza, H.B. Sales, R.M.D.C. Farias, G.D.A. Neves, H.D. L. Lira, R.R. Menezes, A brief review of MoO3 and MoO3-based materials and recent technological applications in gas sensors, lithium-ion batteries, adsorption, and photocatalysis, Materials 16 (24) (2023) 7657.

[32] K. Hosono, I. Matsubara, N. Murayama, S. Woosuck, N. Izu, Synthesis of polypyrrole/MoO3 hybrid thin films and their volatile organic compound gas-sensing properties, Chem. Mater. 17 (2) (2005) 349–354.

[33] B. Mandal, M. Das, M.T. Htay, S. Mukherjee, Architecture tailoring of MoO3 nanostructures for superior ethanol sensing performance, Mater. Res. Bull. 109 (2019) 281–290.

[34] S. Bai, S. Chen, L. Chen, K. Zhang, R. Luo, D. Li, C.C. Liu, Ultrasonic synthesis of MoO3 nanorods and their gas sensing properties, Sensors Actuators B Chem. 174 (2012) 51–58.

[35] Q.N. Abdullah, A.R. Ahmed, A.M. Ali, F.K. Yam, Z. Hassan, M. Bououdina, Novel SnO2-coated β-Ga2O3 nanostructures for room temperature hydrogen gas sensor, Int. J. Hydrog. Energy 46 (9) (2021) 7000–7010.

[36] S. Pandey, G.K. Goswami, K.K. Nanda, Nanocomposite based flexible ultrasensitive resistive gas sensor for chemical reactions studies, Sci. Rep. 3 (1) (2013) 2082.

[37] F.H. Alkallas, A. Ben Gouider Trabelsi, M. Shkir, S. AlFaify, Enhanced room temperature ammonia gas sensing properties of Fe-doped MoO3 thin films fabricated using nebulizer spray pyrolysis, Nanomaterials 12 (16) (2022) 2797.

[38] E. Vinoth, N. Gopalakrishnan, Fabrication of interdigitated electrode (IDE) based ZnO sensors for room temperature ammonia detection, J. Alloys Compd. 824 (2020) 153900, https://doi.org/10.1016/j.jallcom.2020.153900.

[39] S. Kumar, A. Singh, R. Singh, S. Singh, P. Kumar, R. Kumar, Facile h-MoO3 synthesis for NH3 gas sensing application at moderate operating temperature, Sensors Actuators B Chem. 325 (2020) 128974, https://doi.org/10.1016/j.snb.2020.128974.

[40] M.N. Talwar, M.M. Kumar, B.R. Sweekar, G. Akshatha, A.G. Prakash, Impact of humidity on hydrothermally synthesised gallium oxide nanoparticles for ammonia gas sensing at room temperature, Mater. Sci. Eng. B 317 (2025) 118195.

[41] Z. Wu, Z. Chen, Z. Deng, N. Dai, Y. Sun, M. Ge, A high-performance room-temperature NH 3 gas sensor based on WO 3/TiO 2 nanocrystals decorated with Pt NPs, RSC Adv. 14 (17) (2024) 12225–12234.

[42] S. Cai, Q. Zhang, C. Chen, J. Wang, B. Lin, X. Liu, L. Chen, A chemiresistive room temperature ammonia gas sensor based on self-assembled PPy/Zntpp, Sensors Actuators B Chem. 399 (2024) 134862, https://doi.org/10.1016/j.snb.2023.134862.

[43] N. Rekha Pilliadugula, Gopalakrishnan., Room temperature ammonia sensing performances of pure and Sn doped β-Ga2O3, Mater. Sci. Semicond. Process. 135 (2021) 106086, https://doi.org/10.1016/j.mssp.2021.106086.

[44] S. Singh, J. Deb, U. Sarkar, S. Sharma, MoS2/WO3 nanosheets for detection of ammonia, ACS Appl. Nano Mater. 4 (3) (2021) 2594–2605, https://doi.org/10.1021/acsanm.0c03239.

[45] N.N. Yakovlev, A.V. Almaev, V.I. Nikolaev, B.O. Kushnarev, A.I. Pechnikov, S. I. Stepanov, A.V. Chikiryaka, R.B. Timashov, M.P. Scheglov, P.N. Butenko, D. A. Almaev, E.V. Chernikov, Low-resistivity gas sensors based on the In2O3-Ga2O3 mixed compounds films, Mater Today Commun 34 (2023) 105241, https://doi.org/10.1016/j.mtcomm.2022.105241.

[46] M. Won, J. Sim, G. Oh, M. Jung, S.P. Mantry, D.-S. Kim, Fabrication of a Fully Printed Ammonia Gas Sensor Based on ZnO/rGO Using Ultraviolet–Ozone Treatment, Sensors 24 (5) (2024) 1691, https://doi.org/10.3390/s24051691.

[47] A. Chithambararaj, A.C. Bose, Hydrothermal synthesis of hexagonal and orthorhombic MoO3 nanoparticles, J. Alloys Compd. 509 (31) (2011) 8105–8110.

[48] Y. Zhao, R.L. Frost, Raman spectroscopy and characterisation of α-gallium oxyhydroxide and β-gallium oxide nanorods, Journal of Raman Spectroscopy: An International Journal for Original Work in all Aspects of Raman Spectroscopy, Including Higher Order Processes, and also Brillouin and Rayleigh Scattering 39 (10) (2008) 1494–1501.

[49] M. Wen, X. Chen, Z. Zheng, S. Deng, Z. Li, W. Wang, H. Chen, In-plane anisotropic Raman spectroscopy of van der Waals α-MoO3, J. Phys. Chem. C 125 (1) (2020) 765–773.

[50] M. Dieterle, G. Mestl, Raman spectroscopy of molybdenum oxides part II. Resonance Raman spectroscopic characterization of the molybdenum oxides Mo 4 O 11 and MoO2, Phys. Chem. Chem. Phys. 4 (5) (2002) 822–826.

[51] M.B. Ghasemian, Y. Wang, F.M. Allioux, A. Zavabeti, K. Kalantar-Zadeh, Coating of gallium-based liquid metal particles with molybdenum oxide and oxysulfide for electronic band structure modulation, Nanoscale 15 (12) (2023) 5891–5898.

[52] X.M. Jiang, Y.X. Liu, S.S. Kan, M.K. Jiang, S.X. Deng, Z.K. Ren, C.B. Yao, Electron transfer mechanism and nonlinear optical properties of Ga2O3/MoS2 Nano heterostructures: implications for optoelectronic devices, ACS Appl. Nano Mater. 7 (9) (2024) 10068–10078.

[53] P.R. Jubu, F.K. Yam, Influence of growth duration and nitrogen-ambient on the morphological and structural properties of beta-gallium oxide micro-and nanostructures, Mater. Chem. Phys. 239 (2020) 122043.

[54] E. Amdeha, R.A. El-Salamony, A.M. Al-Sabagh, Enhancing the photocatalytic activity of Ga2O3–TiO2 nanocomposites using sonication amplitudes for the degradation of rhodamine B dye, Appl. Organomet. Chem. 34 (2) (2020) e5336.

[55] G. Sinha, D. Ganguli, S. Chaudhuri, Crystallization and optical properties of finite sizedβ-Ga2O3 in sol–gelderived Ga2O3: SiO2 nanocomposites, J. Phys. Condens. Matter 18 (49) (2006) 11167.

[56] A. Almasbek, A. Kozlovskiy, M.V. Zdorovets, The effect of doping with gallium and indium oxides on the optical and shielding characteristics of 0.5 TeO2-(0.5-2x) MoO3-xGa2O3-xIn2O3 glasses, Opt. Mater. 118 (2021) 111271.

[57] X. Du, Z. Li, C. Luan, et al., Preparation and characterization of Sn-doped b-Ga2O3 homoepitaxial films by MOCVD, J. Mater. Sci. 50 (2015) 3252–3257, https://doi.org/10.1007/s10853-015-8893-4.

[58] M. Fan, Y. Lu, K. Xu, Y. Cui, L. Cao, X. Li, Growth and characterization of Sn-doped b-Ga2O3 thin films by chemical vapor deposition using solid powder precursors toward solar blind ultraviolet photodetection, Appl. Surf. Sci. 509 (2020) 144867, https://doi.org/10.1016/j.apsusc.2019.144867.

[59] R. O'Donoghue, J. Rechmann, M. Aghaee, et al., Low temperature growth of gallium oxide thin films via plasma enhanced atomic layer deposition, Dalton Trans. 46 (2017) 16551–16561, https://doi.org/10.1039/c7dt03427j.

[60] J. Tao, H. Lu, Y. Gu, et al., Investigation of growth characteristics, compositions, and properties of atomic layer deposited amorphous Zn-doped Ga2O3 films, Appl. Surf. Sci. 476 (2019) 733–740, https://doi.org/10.1016/j.apsusc.2019.01.177.

[61] D. Guo, H. Liu, P. Li, et al., Zero-power-consumption solar-blind photodetector based onb-Ga2O3/NSTO heterojunction, ACS Appl. Mater. Interfaces 9 (2017) 1619–1628, https://doi.org/10.1021/acsami.6b13771.

[62] Y. Liao, S. Jiao, S. Li, et al., Effect of deposition pressure on the structural and optical properties of Ga2O3 films obtained by thermal post-crystallization, Cryst Eng Comm 20 (2018) 133–139, https://doi.org/10.1039/c7ce01567d.

[63] S.K.S. Patel, K. Dewangan, N.S. Gajbhiye, Synthesis and room temperature d0 ferromagnetic properties of α-MoO3 nanofibers, J. Mater. Sci. Technol. 31 (2015) 453–457, https://doi.org/10.1016/j.jmst.2014.08.013.

[64] Y. Nerthigan, A.K. Sharma, S. Pandey, K.H. Sharma, M. Shahnawaz Khan, D. R. Hang, H.F. Wu, Glucose oxidase assisted visual detection of glucose using oxygen deficient α-MoO3-x nanoflakes, Microchim. Acta 185 (2018) 3–10, https://doi.org/10.1007/s00604-017-2612-6.

[65] P.S. Kumar, L. Korving, K.J. Keesman, M.C. van Loosdrecht, G.J. Witkamp, Effect of pore size distribution and particle size of porous metal oxides on phosphate adsorption capacity and kinetics, Chem. Eng. J. 358 (2019) 160–169.

[66] L. Vradman, M.V. Landau, D. Kantorovich, Y. Koltypin, A. Gedanken, Evaluation of metal oxide phase assembling mode inside the nanotubular pores of mesostructured silica, Microporous Mesoporous Mater. 79 (1–3) (2005) 307–318.

[67] A. Huang, Y. He, Y. Zhou, Y. Zhou, Y. Yang, J. Zhang, J. Yang, A review of recent applications of porous metals and metal oxide in energy storage, sensing and catalysis, J. Mater. Sci. 54 (2) (2019) 949–973.

[68] Y. Zhao, R.L. Frost, W.N. Martens, Gallium-doped boehmite nanotubes and nanoribbons. A TEM, EDX, XRD, BET, and TG study, J. Phys. Chem. C 111 (14) (2007) 5313–5324.

[69] B.R. Sivasankaran, M. Balaji, Novel gallium oxide/reduced graphene oxide nanocomposite for ammonia gas sensing application, Mater. Lett. 288 (2021) 129386.

[70] X.V. Le, T.L.A. Luu, H.L. Nguyen, C.T. Nguyen, Synergistic enhancement of ammonia gas-sensing properties at low temperature by compositing carbon nanotubes with tungsten oxide nanobricks, Vacuum 168 (2019) 108861.

[71] J. Lee, B.T. Nguyen, D. Nguyen, J. Kim, J. Kim, T.B. Phan, S.S. Kim, Gas sensing properties of mg-incorporated metal–organic frameworks, Sensors 19 (15) (2019) 3323, https://doi.org/10.3390/s19153323.

[72] H. Tai, Z. Duan, Y. Wang, S. Wang, Y. Jiang, Based sensors for gas, humidity, and strain detections: A review, ACS Appl. Mater. Interfaces 12 (28) (2020) 31037–31053.

[73] R. Pilliadugula, N.G. Krishnan, Effect of pH dependent morphology on room temperature NH3 sensing performances of β-Ga2O3, Mater. Sci. Semicond. Process. 112 (2020) 105007, https://doi.org/10.1016/j.mssp.2020.105007.

[74] R. Pandeeswari, B.G. Jeyaprakash, High sensing response of β-Ga2O3thin film towards ammonia vapours: influencing factors at room temperature, Sensors Actuators B 195 (2014) 206, https://doi.org/10.1016/j.snb.2014.01.025.

[75] Y. Zhang, M.Y. Wang, X.G. San, Y.B. Shen, G.S. Wang, L. Zhang, D. Meng, Ti3C2T x/SnO2 P–N heterostructure construction boosts room-temperature detecting formaldehyde, Rare Metals 43 (1) (2024) 267–279.

[76] J.Y. Hu, H. Lei, H.Y. Zhang, X.X. Xue, X.P. Wang, C.H. Wang, Y. Zhang, High reliable gas sensor based on crystal-facet regulated α-Fe2O3 nanocrystals for rapid detection of exhaled acetone, Rare Metals 43 (12) (2024) 6500–6515.

[77] Y.X. Wang, B. Liu, B.H. Liu, Y. Zhang, Oxygen-assisted recoverable hydrogen sensor based on sensing gate field effect transistor with ppb-level detection ability, Rare Metals 44 (2) (2025) 1160–1169.

[78] S.S. Sunu, E. Prabhu, V. Jayaraman, K.I. Gnanasekar, T.K. Seshagiri, T. Gnanasekaran, Electrical conductivity and gas sensing properties of MoO3, Sensors Actuators B Chem. 101 (1–2) (2004) 161–174.

[79] R.G. Pavelko, H. Daly, C. Hardacre, A.A. Vasiliev, E. Llobet, Interaction of water, hydrogen and their mixtures with SnO2 based materials: the role of surface hydroxyl groups in detection mechanisms, Phys. Chem. Chem. Phys. 12 (11) (2010) 2639–2647.